Proceedings of International Conference on Heat Exchanger Fouling and Cleaning - 2011 (Peer-reviewed)
June 05 - 10, 2011, Crete Island, Greece
Editors: M.R. Malayeri, H. Müller-Steinhagen and A.P. Watkinson
Published online
www.heatexchanger-fouling.com

FREEZING FOULING CAUSED BY FAT CRYSTALLISATION ON COOLED SURFACES

J-Y. Huang[1], Y.M.J. Chew[2] and D.I. Wilson[1]

[1] Department of Chemical Engineering and Biotechnology, University of Cambridge, New Museum Site, Pembroke Street, Cambridge, CB2 3RA, UK and E-mail (D.I. Wilson): diw11@cam.ac.uk
[2] Department of Chemical Engineering, University of Bath, Building 9 West, Claverton Down, Bath, BA2 CAY, UK

ABSTRACT

The rate of growth of freezing fouling deposits is sensitive to surface temperature and shear stress. The novel spinning disk apparatus (SDA) developed by Nigo *et al.* (2009) to study fat (and wax) deposition on chilled surfaces was fitted with a heat flux sensor to monitor the heat flux, surface temperature and deposit thermal resistance in real time. Fouling studies were performed with model solutions of 5 wt% tripalmitin (PPP, the highest melting point component in palm oil) in a paraffin oil in the 'cold start' mode, wherein the experiment starts with the surface colder than the steady state, simulating one mode of operating a standard 'cold finger' experiment. The cold surface promotes the rapid formation of an initial gel layer, followed by a period of linear fouling and finally falling rate fouling behaviour. The linear fouling rate was relatively insensitive to temperature and shear rate. The linear regime terminated when the surface temperature reached a transition temperature (~ 5 K below the melting point). The fouling rate in the falling rate regime was determined by the deposit surface temperature, and the behaviour was found to follow normal growth kinetics. The solids fraction and PPP concentration within the deposit increased over the length of a fouling experiment for all conditions tested.

INTRODUCTION

Fouling is the accumulation of unwanted solids on process surfaces. These materials usually have low thermal conductivity, resulting in a major resistance to heat transfer (Perry and Green, 1997). Deposition can also cause partial or complete blockage of piping and process equipment; reducing flow rate together with increasing pressure drop. Crystallisation fouling covers the group of deposition mechanisms where fouling layers are formed as a result of solubility differences, such that solids appear from solution at the heat transfer or process surface. Epstein (1983) further characterized crystallisation fouling in terms of scaling – that commonly observed in heating aqueous solutions containing inverse solubility salts such as calcium carbonate – and freezing fouling, wherein a deposit is formed on a sub-cooled surface via solidification of a (pure) melt or the higher melting point constituents of a solution.

The formation of waxes in subsea oil pipelines (*e.g.* Singh *et al.*, 2000) is an important example of freezing fouling. Analogous phenomena exist in the food sector: the formation of wall deposits can be a major problem in pipes distributing food fats. This 'coring' is caused by higher melting point components crystallizing from solution to form a viscous gel which hardens over time. Food fats, like waxy crude oils, are multi-component mixtures, which form crystals when their temperature falls below the cloud point, T_c: this is defined as the temperature at which the first visible solid particles appear in a fluid. Spontaneous, homogeneous, crystallisation is improbable in the metastable region between the melting and cloud points. Nucleation is a kinetic process, however, and a crystal seed or foreign surface can promote heterogeneous nucleation and growth in this region (Mullin, 1993). The general scenario for crystallisation is that the solution must firstly reach supersaturation, followed by nucleation and orientation of crystallites ending up with aggregation and growth of the crystals (Hartel, 2001). The controlling step in deposit growth is largely unknown, and key mechanisms, whether normal growth (Jackson and Chalmers, 1956), two-dimensional nucleation (Hillig, 1966) or screw dislocation (Hillig and Turnbull, 1956), remain to be identified.

Several studies have been undertaken to improve the understanding of freezing fouling processes (Bott, 1997). Whereas studies of fouling on heated surfaces can often be performed under conditions of constant heat flux or constant wall temperature, the practical difficulties in achieving constant local heat fluxes in cooling (requiring evaporation or large Peltier devices) mean that most experiments are performed with a constant overall temperature driving force. As deposit grows, the solution-deposit temperature increases and the driving force for deposition decreases. Fouling resistance-time (R_f - t) plots usually exhibit falling rate or asymptotic fouling behaviour (Epstein, 1983) and can often be fitted to the Kern-Seaton (1959) model, even though this model attributes the observed retardation to increased 'removal' as the deposit grows.

Freezing fouling may occur at rest, such as in a reservoir, or under conditions of high shear rate and large temperature gradients, as in a scraped surface heat exchanger. For this reason, several studies have been

undertaken to investigate the effect of thermo-mechanical history on fouling behaviour.

The temperature difference between the bulk liquid and the cold wall is generally regarded as the thermal driving force for deposition. (Bidmus and Mehrotra, 2004) reported an increase in wax deposition from oils with an increase in the temperature difference across the deposit layer. Increasing the flow rate may cause deposit removal because of the higher shear force. Other studies (Singh *et al.*, 2000) have shown that with constant temperature differential between the crude oil and deposition surface, the deposit thickness decreased as the Reynolds number was increased under both laminar and turbulent flow conditions.

Recently, (Nigo *et al.*, 2009) reported the design and operation of a novel spinning disc apparatus (SDA) featuring a cooled, rotating, vertical cylinder which operates in the laminar flow regime. Deposition occurs on the cold, removable base (the sides are insulated). The geometry and flow conditions mean that mass and heat transfer fluxes to the surface are uniform over the disc surface (Grant *et al.*, 1996; Huang, 2010), making experimental results simpler to interpret. Spinning disc devices have been used to study heat-induced fouling (Rosmaninho and Melo, 2006) and cleaning (Grant *et al.*, 1996), but chilled systems are rare. The advantages and drawbacks of those apparatuses has been summarized by Huang (2010).

In this paper, the SDA is used to study freezing fouling with model solutions of 5 wt% tripalmitin (PPP) in a paraffin oil, similar to those used by Fitzgerald *et al*. (2004). Series of experiments were performed to study the effects of deposition time, disc rotation speed and temperature driving force on fouling behaviour. A heat flux sensor located in the SDA allows the change in local thermal fouling resistance, R_f, to be monitored. The rate of change of R_f can be compared with quantitative crystallisation theory and the underlying kinetics investigated. The deposit gels were weighed and analysed to track any changes in composition which could be related to ageing (Singh *et al*., 2001).

MATERIALS & METHODS

Spinning disc apparatus

Figure 1 shows a schematic of the SDA: a detailed description is given in (Nigo *et al.*, 2009). Briefly, the apparatus consists of a rotating cylindrical can connected to a coolant unit which circulates a water/glycol mixture. The can is positioned within a jacketed vessel holding the fat solution. The can sides are insulated so that heat transfer occurs through the base. Warm water is circulated through the jacket to regulate the bulk solution temperature. A stirrer located at the bottom of the jacketed vessel provides stirring and maintains temperature uniformity in the bulk solution.

Figure 2 shows the arrangement of the fouling test plate which was also employed in heat transfer studies. A micro-foil heat flux sensor (Rhopoint, UK, type 27160) was located between a brass block and a removable 316 stainless-steel disc to measure the local heat flux. A description of experiments characterising the heat transfer performance of SDA is given in (Huang *et al.*, 2010). The results (data not reported here) indicated that SDA was performing as expected for a spinning disc.

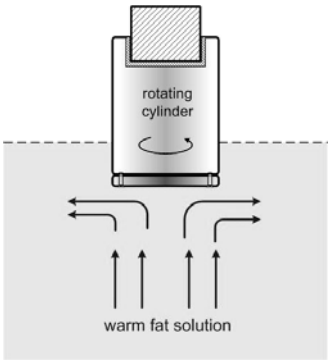

Fig. 1 Schematic of the operation of the SDA

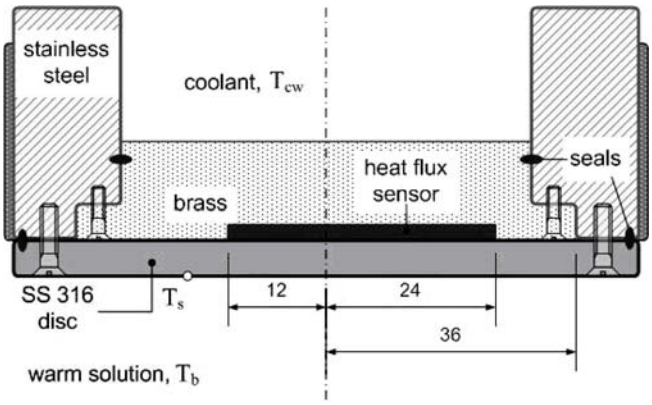

Fig. 2 Construction of the fouling cell plate. Dimensions are in millimeters (not to scale).

Since surface temperature and shear stress are key parameters in freezing fouling, experimental investigations of the SDA heat transfer performance were combined with computational fluid dynamics simulation studies to generate maps of the temperature and shear stress conditions on the SDA surface. Both of these parameters are sensitive to the rotational speed, while the former is more sensitive to the overall temperature difference. The results confirmed that the disc thermal resistance was small and heat transfer was controlled by the bulk fluid (Huang *et al.*, 2011).

Fat Deposition Studies

Model solutions were prepared from tripalmitin (PPP), the highest melting component in palm oil, in a non-crystallising paraffin solvent. The PPP (>85% purity; density, 1480 kg m^{-3}, Sigma Chemicals, UK) was dissolved in paraffin (density at 25 °C, 870 kg m^{-3}; thermal conductivity, 0.15 W m^{-1} K^{-1}, BDH Chemicals, UK) to give solution concentrations of 5 wt%. Other concentrations are currently being studied. The solution melting point, T_m, (*i.e.* the temperature at which the solid and liquid phase exist in equilibrium) of 49.1 °C, was determined by

differential scanning calorimetry. The cloud point, T_c, being the temperature at which crystals are first detected on cooling the solution (at cooling rate 0.5 K min^{-1}), was measured as 29.8 °C with an ODEON turbidity meter.

2 L test solution was charged into the reservoir, which was heated to the bulk temperature, T_b, 60 °C, by circulating hot water through the heating jacket. Deposition experiments reported here were performed in a 'cold start' mode, wherein the can was initially isolated from the reservoir and attained the coolant temperature before being lowered into the solution and rotation started. The heat transfer data therefore exhibited an initial transient on immersion of the cooled plate into the warm solution. This was studied separately using PPP-free paraffin solution, which showed that the transient lasted up to one minute.

The rotational speeds, ω_d, used were 2.2, 3.5, 5.4 and 7.3 rad s^{-1}, corresponding to rotational Reynolds numbers of 26, 41, 64 and 86, respectively. Coolant temperatures, T_{cw}, used were 9.8 °C (*i.e.* $T_c - 20$), 19.8 °C ($T_c - 10$), 24.8 °C ($T_c - 5$) and 29.8 °C (T_c). Fouling experiments were normally run for 12 h, but a series of interrupted experiments were run at identical conditions, at 1, 3, 6, 9 and 12 hr. The final deposit was removed from the surface using a plastic spatula, weighed and stored for further analysis.

Calculation of fouling resistance

The heat flux, q, through the rotating disc at any point is given by Newton's law of cooling;

$$q = U(T_b - T_{cw}) = h_b(T_b - T_s) \quad (1)$$

and the overall heat transfer coefficient, U, is given by;

$$\frac{1}{U} = \frac{1}{h_b} + R_{cw} + R_w + R_f \quad (2)$$

U is obtained from the SDA experiments. The thermal resistance of disc wall, R_w, is constant. The film heat transfer coefficient in bulk fluid, h_b, and the thermal resistance of coolant side, R_{cw}, can be extracted from the CFD simulations combined with further calculation (Huang *et al.*, 2011). The fouling resistance, R_f, is calculated from

$$R_f(t) = \frac{1}{U(t)} - \frac{1}{U_0} \quad (3)$$

where U_0 is the initial, clean, overall heat transfer coefficient.

Deposit Analysis

The deposits consisted of particulate gels of PPP crystals in a liquid matrix. Gas chromatography (GC) analysis of deposit samples dissolved in *n*-heptane yielded the total PPP content, C_T: this was conducted on a Hewlett Packard Agilent 6890 GC equipped with a dimethylpolysiloxane column (10 m × 0.32 mm × 0.1 µm) and a flame ionisation detector using helium as the carrier gas. The GC was calibrated and programmed using the BS EN 14105:2003 method.

The solids content of the deposit was determined by filtration. About 3 g of deposit was loaded on to a 0.2 µm polytetrafluoroethylene membrane filter paper (Cole-Parmer, USA) and vacuum applied. The filtered solids were washed with hexane (analytical reagent grade, Fisher Scientific, UK) at ambient temperature to remove any entrained paraffin followed by acetone to remove traces of hexane, then allowed to dry at room temperature for an hour before weighing.

Statistical analysis

Analysis of variance (ANOVA) was applied to analyse the influence of deposition time, rotational speed and coolant temperature on deposit composition and, when the effect of the factors was significant ($p < 0.05$), the Fisher's least significant difference (LSD) test was used (95% confidence level).

RESULTS & DISCUSSSION

Effect of deposition time on fouling

Fouling experiments involved measurement of heat flux and temperature with deposition time, t_d. The reproducibility of the fouling experiments ~~test~~ was confirmed by conducting a series of experiments under identical conditions for various t_d. The R_f - t_d profiles in Figure 3 show good agreement, with a maximum difference of 3%. Experiments were repeated only when the results were inconsistent with observed trends. This series of experiments also allowed the evolution of deposit properties to be investigated.

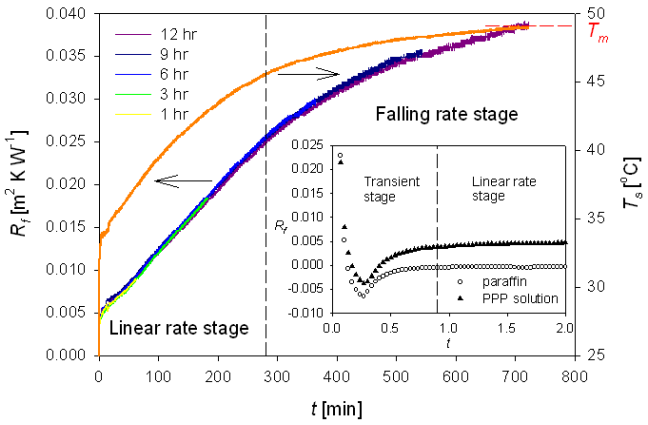

Fig. 3 Thermal resistance and estimated interface temperature during fouling of 5 wt% PPP solutions at T_{cw} = 9.8 °C, ω_d = 5.4 rad s^{-1}. Vertical dashed line separates linear rate stage from the falling rate stage. Inset shows initial transients for PPP solution and for solvent alone, t in minutes.

The R_f - t plots obtained in the cold start experiments discussed here all showed similar behaviour, exhibiting three stages:

(*i*) an initial step in R_f,
(*ii*) a period of linear fouling increase, followed by
(*iii*) a falling rate period, where R_f approaches an asymptote.

The initial sharp increase in R_f derives from the cold start mode. On immersion of the test cell, the warm solution is contacted with the cold surface (below T_c), inducing gel formation. At the same time, the heat flow through the cell is larger than at steady state owing to the surface starting cold which generates a temporally large heat flux and associated U value, giving rise to negative R_f values shown in the inset on Figure 3. The thermal steady state was reached within 2 min, by which time a gel layer had been established. This effect declines in relative importance as R_f becomes large. Negative values of R_f associated with roughness enhancing convective heat transfer have been reported by other workers, *e.g.* Bansal *et al.*, (2008); (Bansal and Muller-Steinhagen, 1993) but this transient mechanism is rarely reported, mainly because the experiments start with heat transfer in steady state.

In the subsequent stages, as deposit accumulates, the deposit-solution interface temperature, T_s, increases and subcooling (the driving force for growth) decreases. T_s was estimated from combining of eqs (1) and (2) to give:

$$T_s(t) = T_b - \frac{q}{h_b} = T_b - \left[\frac{T_b - T_{cw}}{R_{cw} + R_w + R_f(t) + \frac{1}{h_b}} \right] \frac{1}{h_b} \qquad (4)$$

Figure 3 shows a rapid increase in T_s which then slows down and a gradual approach to the melting point temperature, T_m. The value of h_b was extracted from CFD simulations, reported elsewhere (Huang *et al.*, 2011). Other experiments showed this behaviour and indicated that deposit growth continued beyond the cloud point into the metastable zone.

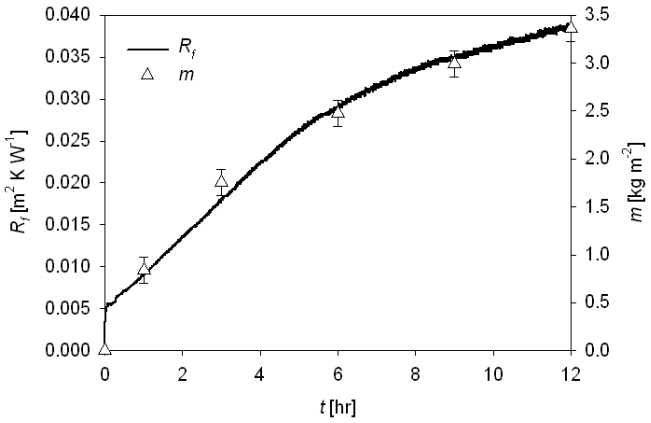

Fig. 4 Comparison of deposit mass and fouling resistance for experiments ~~tests~~ reported in Figure 3.

Figure 4 shows that the increase in deposit mass matched the thermal fouling resistance, indicating that the heat flux measurements provided a reliable monitor of deposit growth, *i.e.* deposition was relatively uniform. The relationship between R_f and the mass of deposit per unit disc surface, m, is;

$$R_f = \frac{m}{\rho k} \qquad (5)$$

where ρ is the deposit density. The deposit thermal conductivity, k, was taken to be 0.15 W m^{-1} K^{-1}, as the thermal conductivity of solid PPP is conveniently close to that of paraffin. The plot of the thermal parameter R_f against the measured mass m in Figure 5 shows a linear relationship (R^2 = 0.97), in good agreement with equation (5). The gradient of 0.011 m^4 K W^{-1} kg^{-1}, gives ρk = 91 W kg m^{-4} K^{-1}, which is lower than that ρk for the oil, 130.5 W kg m^{-4} K^{-1}. ρk for the PPP solids will be greater again. The difference may be due to the difficulty in collecting all the deposit (affecting m), and any systematic errors in evaluating R_f. The linear relationship does, moreover, indicate that the age of the deposit does not affect heat transfer (*e.g.* by changing k). Figure 5 also shows the data obtained from other experiments conducted in this study: all show good agreement with the above trend.

The concentration of PPP in the liquid phase present in the deposit, C_S, is calculated from the measured values of C_T (GC) and C_X (filtration) via

$$C_S = \frac{C_T - C_X}{100 - C_X} \qquad (6)$$

The deposit composition results in Figure 6 show noticeable changes over the course of the fouling run. The solids content increased – almost linearly – to about 15 wt% over the first 6 hr, coinciding with the linear increase in R_f. The subsequent change in C_X was less marked, reaching 20 wt% after 12 hr. It was not possible here to determine the local solids distribution: this will be investigated using freezing techniques.

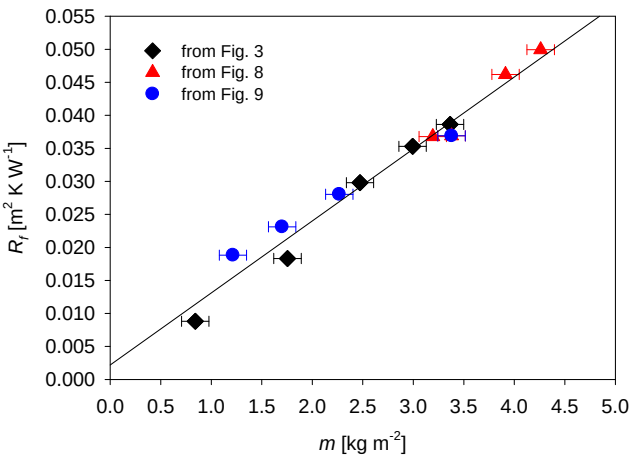

Fig. 5 Correlation of thermal resistance and deposit mass for fouling runs in Figures 3, 8 and 9.

Figure 6 shows that C_S is initially close to the bulk liquid concentration and increases with time to around 10 wt%. The increase in C_S is less marked than that in C_X. This enrichment of the matrix solution over time could be

explained by diffusion, driven by secondary solidification in the deposit layer, or by shear-induced hardening. The latter is related to the shear stress imposed on the SDA surface: the stress is controlled by the operation speed, liquid properties and surface temperature. As the surface temperature increases, the viscosity of the liquid phase decreases and the solids content required to form a gel strong enough to resist deformation by the surface shear stress will increase. These competing aspects of temperature have been reported for wax formation in crude oils by (Jennings and Weispfennig, 2005). Decoupling these factors is the subject of ongoing work, including rheological testing of the deposit gels. Shear hardening would not require C_S to increase. It should also be noted that the variation in C_S beyond 6 hr was not statistically significant.

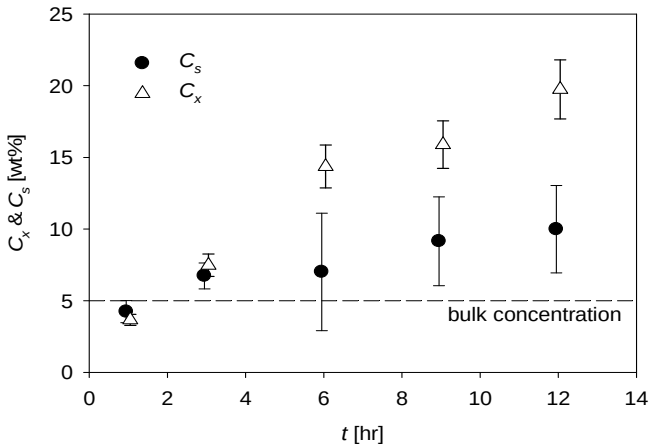

Fig. 6 Evolution of deposit composition for deposits in Figure 3.

Growth rates

Deposit growth can be considered to arise from attachment of molecules to the existing surface, attachment of particulates, or secondary nucleation in the gel. In each case the local growth rate will vary with temperature driving force. No particulates were present in the solutions. The thickness growth rate, $G(T)$, can be calculated from the fouling resistance measurements by assuming the deposit thickness, δ_f, is uniform and k is known, *via*

$$G(T) = \frac{d\delta_f}{dt} = k\frac{dR_f}{dt} \qquad (7)$$

In crystallisation studies, the growth rate is often related to the temperature driving force, and ΔT, being the difference between the equilibrium melting temperature, T_m, and the temperature of crystallisation, here T_s. The gradient in equation (7) and ΔT were evaluated in the falling rate stage by interpolating the R_f and T_s data and extracting values at particular points. Figure 7 shows the results obtained for the runs in Figure 3. A linear trend is evident, which is the form expected for normal growth (Borisov *et al.*, 1969):

$$G(T) = K\Delta T \qquad (8)$$

The fitted line does not pass through the origin, which is attributed to the systematic uncertainties involved in calculating T_s from the experimental data. The corresponding plots for growth by secondary nucleation (plotting G *vs* $T_s\Delta T$; Borisov *et al.*, 1968) did not show good agreement.

Effect of velocity/shear rate

The effect of shear rate was studied at four can rotational speeds, corresponding to average shear stresses on the disc surface of 0.26, 0.52, 1.03 and 1.66 Pa. Figure 8(*a*) presents the R_f - t profiles obtained from experiments performed at T_{cw} = 9.8 °C for 12 hr. The three stages described previously are evident in each case. The initial step increase in R_f decreased as ω_d increased. This may occur because the incipient gel is relatively weak, and was less able to resist the shear forces imposed on it at higher ω_d, or because the new, steady state temperature was warmer at higher rotational speed (Equation (4)).

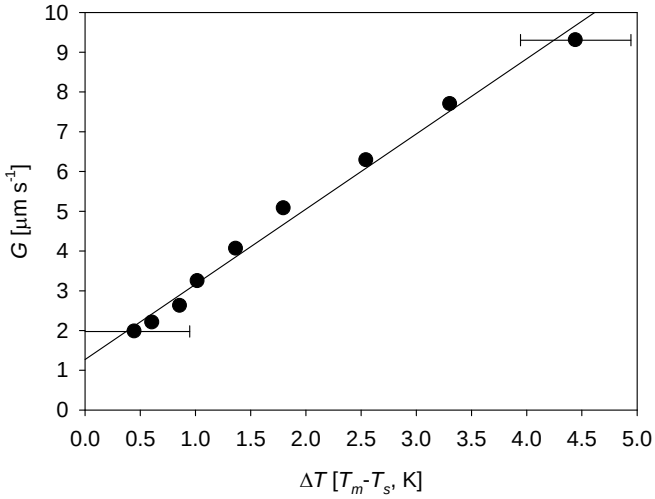

Fig. 7 Growth rate of deposit thickness for fouling runs in Figure 3 showing linear dependence on ΔT. Line shows fit to linear trend.

The linear fouling rate did not change appreciably with ω_d, varying from 1.21×10^{-6} m^2 K J^{-1} to 1.32×10^{-6} m^2 K J^{-1}. Inspection of the estimated T_s - t plots showed that the end of the linear fouling stage occurred at similar values of T_s, around 45.7 ºC (*i.e.* T_m – 4.6 K).

The R_f value reached after 12 hr was greater for lower ω_d, which is consistent with the deposit mass measurements in Figure 8(*b*). The T_s - t plots indicated that the surface temperature approached T_m after 12 hr, confirming that the falling rate fouling behaviour observed was related to surface temperature effects (as in Figure 7).

The deposit composition data in Figure 8(*b*) show a stronger influence of ω_d on solids fraction than matrix solution composition. The variation in C_S lies within the

confidence limits for the hypothesis that the C_S value is the same for all cases. The solids content, C_X, increases with ω_d, by a factor of 3-4× over the range of rotational speeds studied, which is consistent with the deposit being stiffer to withstand the higher shear stress conditions. This could also be explained by the smaller deposit thickness and higher h_b giving a larger temperature gradient across the gel, resulting in a higher diffusive flux for hardening and larger C_X (Singh *et al.*, 2001).

(*a*)

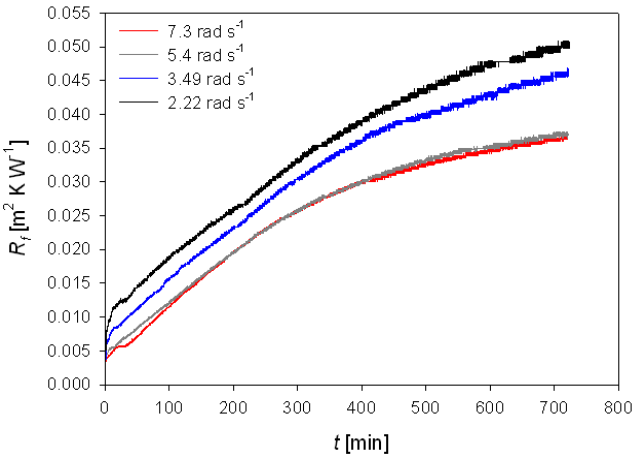

(*b*)

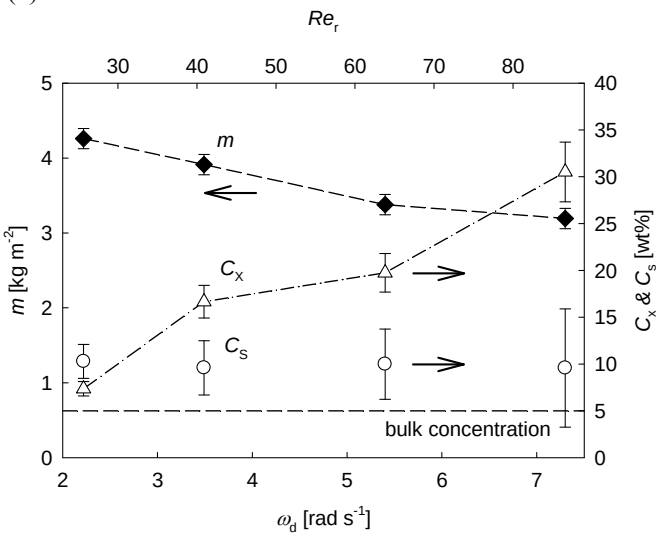

Fig. 8 Effect of rotational speed on (*a*) fouling behaviour and (*b*) final deposit mass and composition. Conditions: T_{cw} = 9.8 °C, t = 12 hr.

Effect of thermal driving force

Figure 9 shows the effect of thermal driving force for experiments performed at ω_d = 5.4 rad s^{-1} with four different coolant temperatures. The Figure legend indicates the degree of subcooling (T_c - T_s). The R_f - t profiles again exhibit the three stages mentioned above. The initial step increase is larger and the final R_f value higher with increased subcooling (lower T_{cw}), as expected.

The linear stage was shorter as T_{cw} increased, which is consistent with less time elapsing before the transition temperature was reached. The linear fouling rates were similar, ranging from 1.04×10^{-6} to 1.21×10^{-6} m^2 K J^{-1}.

The final deposit mass also increased with the degree of subcooling, and Figure 10 suggests a strongly linear relationship. This extrapolated locus continues beyond the cloud point, but experiments were not performed to see if deposit would grow in the timescale of these experiments with $T_{cw} > T_c$.

(*a*)

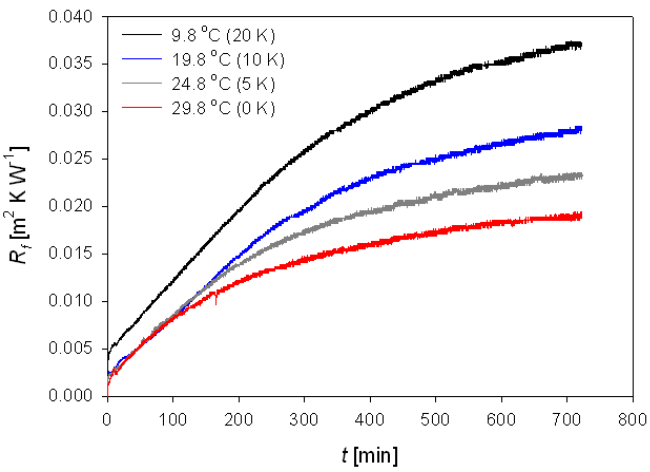

(*b*)

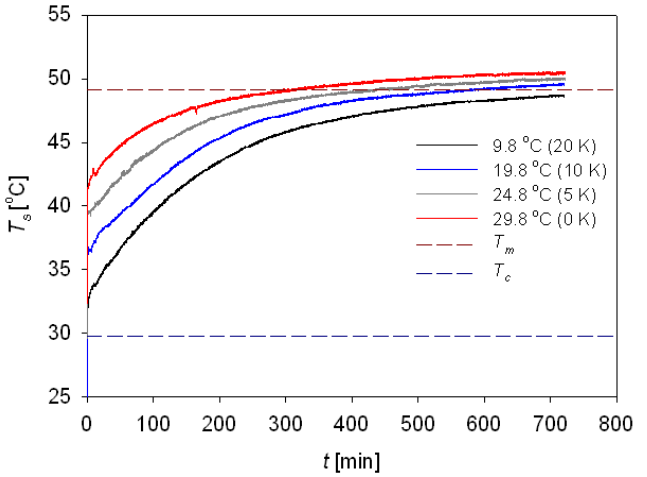

Fig. 9 Effect of coolant temperature on (*a*) fouling behaviour and (*b*) surface temperature profile. Conditions: ω_d = 5.4 rad s^{-1} and t = 12 hr.

The deposit composition data in Figure 10 show little effect of initial subcooling on PPP concentration in the entrained liquid, C_S. The values are consistently larger than the bulk concentration, of 5 wt%. The solids mass fraction C_X increases twofold over the T_{cw} range studied. Visual inspection of the deposits indicated that for a fixed shear rate, those formed at higher coolant temperature (lower degrees of subcooling) were firmer. The faster rate of

deposition (at lower coolant temperature) may contribute to the deposit being able to incorporate more solution (Jennings and Weispfennig, 2005) owing to the higher liquid viscosity at lower temperature.

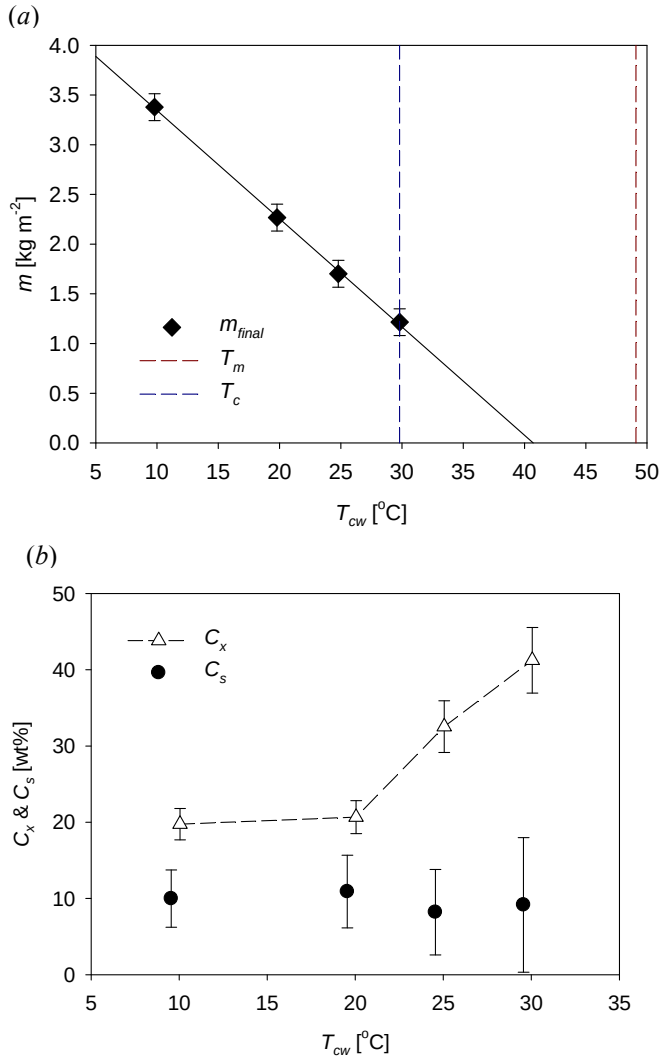

Figure 10 Effect of coolant temperature on deposit (*a*) mass and (*b*) composition, for the fouling runs in Figure 9. Vertical lines in (*a*) indicate the cloud point and melting temperature. Fitted black line drawn as a guide to the eye.

CONCLUSIONS

A series of laboratory experiments were carried out in the modified SDA with a model solution of PPP in a noncrystallising solvent to investigate the effects of changing deposition time, shear and thermal driving force on the crystallisation fouling behaviour of food fats. R_f - t profiles for these 'cold start' experiments exhibited three stages: transient, linear rate and falling rate stage. R_f - t profiles could be generated reliably and reproducibly, indicating that the heat flux measurements provide a reliable monitor of deposit growth. In all cases, the estimated surface temperature increased quickly initially and then levelled off to approach the experimentally measured melting point.

The kinetics (*i.e.* R_f - t_d behaviour) of fat deposit formation was studied. After the initial gel formation, in the linear rate stage the fouling rate was relatively sensitive to both ω_d and ΔT. The fouling rate in the falling rate stage showed a linear relationship to ΔT, regardless of the operating conditions. This latter result is close to the dependence expected for normal growth.

At the same values of ω_d and T_{cw}, m and C_X increased with time, indicating that deposit ageing occurs in the gels over the time scale of the experiments. However, these increases did not change the deposit properties in terms of ρk. Deposition appears to be driven by gel formation at the shear and temperature conditions acting at the surface. Increasing the amount of shear generally decreased m and increased C_X, which may be attributed to the shear removal and the counter diffusion within the deposit, respectively. Likewise, the effect of decreasing T_{cw} (higher degree of subcooling) led to an expected increase in m as well as yielded decreased C_X, which could be explained by the fact that more solution would be trapped within the deposit with increasing thermal driving force due to the faster fouling rate. In summary, ω_d and T_{cw} have significant effects on m and C_X: the results suggest that a higher value of m corresponds to a lower value of C_X and vice versa.

NOMENCLATURE

Roman

C_X	solids content in deposit, wt%
C_S	PPP content of the solution entrained in deposit, wt%
C_T	total PPP content in deposit, wt%
G	growth of deposit thickness, μm s^{-1}
h_b	film heat transfer coefficient in bulk fluid, W m^{-2} K^{-1}
k	deposit thermal conductivity, W m^{-1} K^{-1}
m	mass of deposit per unit disc surface, kg m^{-2}
q	heat flux, W m^{-2}
R_{cw}	thermal resistance of coolant side, m^2 K W^{-1}
R_f	fouling resistance, m^2 K W^{-1}
R_w	thermal resistance of disc wall, m^2 K W^{-1}
T_b	bulk temperature, °C or K
T_c	cloud point, °C or K
T_{cw}	coolant temperature, °C or K
T_m	melting point, °C or K
T_s	deposit-solution interface temperature, °C or K
ΔT	difference between T_m and T_s, K
t_d	deposition time, s, min or hr
U	overall heat transfer coefficient, W m^{-2} k^{-1}
U_0	initial, clean, overall heat transfer coefficient, W m^{-2} K^{-1}

Greek

δ_f	deposit thickness, μm
ρ	deposition density, kg m^{-3}
ω_d	can rotational speed, rad s^{-1}

ACKNOWLEDGEMENTS

Assistance with the GC analysis from Bob Skelton, and travel funding from Jesus College, Cambridge, are both gratefully acknowledged.

REFERENCES

Albert, F., Augustin, W. and Scholl, S. (2011). Roughness and constriction effects on heat transfer in crystallization fouling, *Chem. Eng. Sci*., Vol. 66(3), 499-509.

Bansal, B., Chen, X. D. and Müller-Steinhagen, H. (2008). Analysis of classical deposition rate law for crystallisation fouling. *Chemical Engineering and Processing: Process Intensification*, *47,* 1201-1210.

Bansal, B. and Müller-Steinhagen, H. (1993). Crystallization Fouling in Plate Heat Exchangers. *J. Heat Transfer*, *115,* 584-591.

Bidmus, H. O. and Mehrotra, A. K. (2004). Heat-transfer analogy for wax deposition from paraffinic mixtures. *Industrial & Engineering Chemistry Research*, *43,* 791-803.

Borisov, V. T., Golikov, I. N. and Matveev, Y. E. (1969). Growth of gallium crystals over a wide range of growth rates. *J. Cryst. Growth*, *6,* 72-76.

Bott, T. R. (1997). Aspects of crystallization fouling. *Exp. Therm Fluid Sci.*, *14,* 356-360.

Epstein, N. (1983). Thinking about heat transfer fouling: A 5 x 5 matrix. *HTrEn*, *4,* 43 - 56.

Fitzgerald, A. M., Barnes, J., Smart, I. and Wilson, D. I. (2004). A model experimental study of coring by palm oil fats in distribution lines. *Food Bioprod. Process.*, *82,* 207-212.

Grant, C. S., Perka, A. T., Thomas, W. D. and Caton, R. (1996). Cleaning of solid behenic acid residue from stainless-steel surfaces. *AlChE J.*, *42,* 1465-1476.

Hartel, R. W. (2001). *Crystallization in Foods*, Aspen Publication, Maryland, USA.

Hillig, W. B. (1966). A derivation of classical two-dimensional nucleation kinetics and the associated crystal growth laws. *Acta Metall.*, *14,* 1868-1869.

Hillig, W. B. and Turnbull, D. (1956). Theory of crystal growth in undercooled pure liquids. *J. Chem. Phys.*, *24,* 914.

Huang, J.-Y. (2010). Crystallisation and Gelation Behaviour of Food Fats on Cold Surfaces. Certificate of Post-Graduate Study Dissertation Thesis, University of Cambridge, UK.

Huang, J.-Y., Chew, Y. M. J. and Wilson, D. I., (2010), Experimental studies of food fat fouling using a novel spinning disc apparatus, *Fouling and Cleaning in Food Processing 2010*, Cambridge, UK.

Huang, J.-Y., Chew, Y. M. J. and Wilson, D. I., (2011), Fouling studies of food fat, *11th International Congress on Engineering and Food*, Athens, Greece.

Jackson, K. A. and Chalmers, B. (1956). Kinetics of solidification. *Can. J. Phys.*, *34,* 473-490.

Jennings, D. W. and Weispfennig, K. (2005). Effects of shear and temperature on wax deposition: Coldfinger investigation with a Gulf of Mexico crude oil. *Energy Fuels*, *19,* 1376-1386.

Mullin, J. W. (1993). *Crystallisation*, Butterworth-Heinemann, London, UK.

Nigo, R. Y., Chew, Y. M. J., Houghton, N. E., Paterson, W. R. and Wilson, D. I. (2009). Experimental studies of freezing fouling of model food fat solutions using a novel spinning disc apparatus. *Energy & Fuels*, *23,* 6131-6145.

Perry, R. H. and Green, D. W. (1997). *Perry's Chemical Engineers' Handbook*, McGraw-Hill, New York, USA.

Rosmaninho, R. and Melo, L. F. (2006). The effect of citrate on calcium phosphate deposition from simulated milk ultrafiltrate (SMUF) solution. *J. Food Eng.*, *73,* 379-387.

Singh, P., Venkatesan, R., Fogler, H. S. and Nagarajan, N. (2000). Formation and aging of incipient thin film wax-oil gels. *AlChE J.*, *46,* 1059-1074.

Singh, P., Youyen, A. and Fogler, H. S. (2001). Existence of a critical carbon number in the aging of a wax-oil gel. *AlChE J.*, *47,* 2111-2124.